**Coalescence of cluster beam generated sub-2 nm bare Au nanoparticles and analysis of Au film growth parameters**

*Emanuele Verrelli[1,2,]\*, Irini Michelakaki[1], Nikos Boukos[3], Georgios Kyriakou[4,5], Dimitris Tsoukalas[1]*

[1]Department of Applied Physics, National Technical University of Athens, Heroon Politechniou 9, Zographou (Athens), 15780, Greece.
[2]Department of Physics and Mathematics, University of Hull, Cottingham road, HU67RX, Kingston upon Hull, United Kingdom.
[3]Institute of Nanoscience and Nanotechnology, National Centre for Scientific Research Demokritos, Terma Patriarchou Grigoriou, Aghia Paraskevi, 15310, Greece
[4]European Bioenergy Research Institute, Aston University, Aston Triangle, Birmingham B4 7ET, United Kingdom.
[5] Chemical Engineering and Applied Chemistry, School of Engineering and Applied Sciences, Aston University, Aston Triangle, Birmingham, B4 7ET, UK.

*Corresponding author. E-mail: verrelli@central.ntua.gr, e.verrelli@hull.ac.uk

## Abstract

In this work is presented the growth model for Au films grown on a carbon substrate at room temperature by using as building blocks Au nanoparticles (NPs) with 1.4 nm mean size generated via remote cluster beam synthesis and soft landing on the substrate. The key results highlighted in this work are that 1) the deposited nanoparticles coalesce at substrate level in such a way that the film growth is 3D, 2) newly formed nanoparticles at substrate level are predominantly magic number clusters and 3) coalescensce takes place as soon as two neighboring nanopartciles come closer than a critical distance. The film growth was investigated by TEM as a function of Au load, in the range 0-1.2 $\mu g/cm^2$. Two distinct regimes are identified: the "landing regime" and the "coalescence regime". During the latter the film growth is 3D with a dynamic scaling exponent z of 2.13. Particular attention was devoted to the study of the evolution of the NP population from the moment they are generated with the cluster beam

generator to the moment they land on the substrate and coalesce with other NPs. Our results show that 1) the NPs generated by the cluster beam are heterogeneous in size and are made by more than 95% by Au Magic numbers , mainly $Au_{20}$ and $Au_{55}$ and 2) kinetic processes (coalescence) at substrate level is capable of producing NPs populations made of larger Au magic numbers containing up to several thousands of Au atoms. Experimental and simulation results provide insight into the coalescence mechanism and provide strong evidence that the NPs coalesce when the nearest neighbor distance is below a critical mark. The critical distance is at its minimum 0.4-0.5 nm and it is still unclear whether it is constant or not although the best matching simulation results seem to point to a superlinear dependence from the NP size difference between two neighboring candidate coalescing NPs. The coalescence phenomenon investigated in this work pinpoints the unique self-organization properties of these small Au NPs in creating films with a stable edge-to-edge mean nearest neighbor distance of the order of 1.4 nm..

Keywords: nanoparticles, coalescence, cluster beam, film growth, nearest neighbor.

# 1   Introduction

The synthesis and reactivity of Au nanoparticles (NPs) is receiving substantial attention due to their important physicochemical properties and their potential applications in chemistry, medicine, sensor technology and nanoelectronics [1,2,3,4]. The catalytic properties of Au NP, in particular, have been a topic of continuing research over the past three decades [5,6,7,8,9,10,11]. Au has been shown to be catalytically active for a wide range of important reactions including the low temperature CO oxidation [12], the selective oxidation of alkenes [9,13,14], hydrogen peroxide formation from $O_2$ and $H_2$ [15], cross coupling [16,17] and hydrogenation reactions [18].The size dependent properties of Au NPs [19] has led to the detailed investigation of cluster formation and stability. In this respect, a substantial experimental and theoretical effort has been devoted to understand the underlying properties which lead to stable Au clusters. Of particular interest have been the energetically stable clusters derived from Au magic numbers [20,21,22]. These atomic arrangements are typically formed by the completion of a geometrically perfect structure or by the closing of an electronic shell [23]. Critically, the chemical properties of nanosized clusters depend strongly on both their electronic and physical structure [20]. Therefore, understanding of the underlying mechanism that controls the formation and growth of Au clusters and particularly of magic Au clusters is of major importance both from a fundamental and technical point of view.

The techniques used to fabricate Au NPs layers can be divided in two main classes which rely on i) the deposition of Au thin films or ii) the deposition of pre-formed NPs. The latter is typically achieved by cluster beam generators [24,25,26,27] or by using colloidal NP systems [28]

while the former is achieved by sputtering [29], pulsed laser deposition [30], thermal and e-beam evaporation [31], molecular beam epitaxy [32], electrochemical [33] methods. The main drawback in the fabrication of Au NPs through the growth of thin Au films is the poor control over the NPs size distribution. Furthermore, the NP formation is found to depend strongly on the nature of the substrate and the specific substrate - adsorbate interactions which dominate the kinetics of the overall growth process. [34,35]. Au NP formation through the deposition of Au thin films has been often found to follow the Wolmer-Weber [29] growth mode, leading to the formation of 3D Au nanoislands with irregular or hemispherical shapes. [36,37,38,39]. More spherically shaped Au NPs have been obtained after rapid thermal annealing (RTA) (Wolmer-Weber growth associated with ripening) [34,39] . The thermal treatment of the film, however, is not always desirable or possible as it increases the thermal budget of the sample and introduces the risk of Au contamination of neighboring materials/structures. Contrary to this, deposition of pre-formed NPs using cluster beam generators, as the present work demonstrates, provides superior control over the NPs size distribution, is a room temperature process and leads to more spherically shaped NPs.

The properties of cluster beam generated NPs films have been recently investigated in terms of their mechanical[40,], antimicrobial[41,42], optical[43,] and electrical[44] characteristics. Cavaliere et al. [42] used supersonic cluster beam deposition (SCBD) to deposit antimicrobial Ag nanoparticle films on soda lime glass with high control over the density and the thickness of the film. The Ag films were found to have stable oxidation state and morphology for prolonged periods of time. Peli et al. [40] aslo used SCBD to deposit Ag NPs on sapphire and studied the resulting film morphology, composition, and mechanical properties in the range of $10 - 50$ nm. The obtained films were composed of crystallites of Ag NPs with 6 nm average size and inter NPs voids. Interestingly the authors studied the photoacoustic nanometrology of the deposited

films and found that they can perform very well as hypersonic acoustic cavities up to and beyond the 100 GHz range. Benetti et al [41] used SCBD to study the formation of bi-elemental Ag-Ti antimicrobial films. The Ag-Ti films were obtained by an one-step gas-phase deposition process which formed bi-elemental Janus type particles on the substrate. The resulting films were composed of Ag nano-crystals embedded in amorphous $TiO_2$ via a cluster-in-cluster mixing phase. Minnai et al [43] fabricated stretchable nanocomposite films with mechanically tunable surface plasmon resonance. The films were produced by implantation in a Polydimethylsiloxane substrate of neutral gold nanoparticles aerodynamically accelerated in a supersonic expansion. Borghi et al. [44] investigated the mechanical properties of the same gold-polydimethylsiloxane nanocomposite for flexible electronic applications, demonstrating a tunable Young's modulus depending solely on the amount of metal clusters implanted in the elastomeric matrix..

Regarding the film growth characteristics and how NPs on the substrate interact with each other the literature is still scarce. An interesting example is represented by the work of Celardo et al. [45] who used femtosecond laser ablation deposition in air at ambient conditions to study the fractal nanostructures of titanium dioxide, TiO2, on a variety of substrates. Based on the experimental data and on Monte Carlo simulations the authors have found that the nanostructures are formed after landing of the ablated material on the surface by a diffusion mechanism. For what concerns metallic NPs, examples are represented by the work of Majumdar et al. [46], Divece et al. [47] and Pedersen et al. [48]. Majumdar et al. studied the surface morphology of thin films grown by deposition of 3.4 nm Cu NPs onto Si substrates. The authors found that the soft-landed NPs nucleate upon impact to form nanoclusters, which further coalesce with each other to form larger clusters. Divece et al. examined the evolution of Au NPs with annealing time at 200 ºC on amorphous carbon surfaces. This was done for two different Au NPs populations co-

5

deposited on a carbon substrate by combining the cluster beam generator to a mass selection device. The clusters produced by this method were $Au_{330}$ (1.9 nm diameter and $3\ 10^{11}$ cm$^{-2}$ density) and $Au_{10000}$ (6.7 nm diameter and $3\ 10^{10}$ cm$^{-2}$ density) Interestingly, the size of the $Au_{330}$ clusters was found to be smaller than the one expected from the spherical cluster approximation, suggesting that small Au NPs tend to be faceted. Subsequent annealing studies at temperatures as low as 200 C show that $Au_{330}$ NPs are more mobile and coalesce with the bigger $Au_{10000}$. Pedersen et al. investigated the conductivity of monodisperse 6.5 nm Ag NPs deposited by combining the cluster beam generator to a mass selection device for increasing nominal areal density. The authors show that Ag NPs naturally coalesce as soon as the nearest neighbor distance (edge-to-edge) becomes smaller than 3.5 nm and ascribe this effect to spontaneous charge transfer between neighboring NPs. This limit distance also serves as the border value that separates highly conductive percolation regime from the highly resistive tunneling regime.

The results presented in this work are aimed at understanding the Au film growth kinetics of sub-2 nm Au NPs soft landing on an amorphous carbon film. Carbon surfaces have unique physicochemical properties which makes them attractive for the study of molecular and nanocluster self-assembly. The low cost of carbon and its conductivity properties makes it a desirable material for a variety of applications including industrial scale electrodes, molecular electronics, fuel cell components, bio- and chemical sensors and high surface area supports for industrial catalysts [49]. Furthermore, in the case of Au NPs deposition, the amorphous carbon substrate ensures that the NPs remain stable as it has also been observed for graphene substrates [50]. Particular attention is devoted to the study of the evolution of the NP population from the moment the NPs are generated by the cluster beam generator to the moment they land on the substrate surface and coalesce with other NPs. This approach allowed the identification of

6

several Au magic numbers, some created directly by the cluster beam generator (e.g. $Au_{55}$) and others formed through kinetic processes (coalescence) taking place on the substrate upon NP deposition ($Au_{561}$). This is the first report on the growth of Au magic numbers in the 1.5-3.5 nm range by the coalescence of soft-landing clusters fabricated at room temperature by using cluster beam synthesis.

## 2   Experimental

The NP deposition was performed using a special dc sputtering chamber (NanoGen, Mantis deposition Ltd) attached, through a small aperture, to the main chamber where the sample was located as shown in Figure 1, more details can be found elsewhere [51]. The substrates used in this experiment were carbon films on copper transmission electron microscopy (TEM) grids used as received (C film of 5-6 nm on Cu grid from Electron Microscopy Sciences, type CF200-Cu). The TEM grids substrates were placed into the main chamber 50 cm away from the cluster beam aperture (diameter of 5mm) and kept at room temperature during depositions. A pure Au target (diameter 2", thickness 1/8") was used at a sputtering power of 30 W with an Ar flow of 75 sccm. The DC magnetron head was cooled via a continuous flow of water at 18 C. The pressure inside the main chamber was around $2 \ 10^{-3}$ mBar while the estimated pressure within the aggregation chamber of the cluster beam generator was in the range $10^{-1}$-$10^{-2}$ mBar. By varying the deposition time it was possible to vary the NP film load in the range 0-1 $\mu g/cm^2$ and fabricate in such a way 4 different samples, A to D, with increasing NP load as shown in Table 1. A fifth sample with a very small NP load to avoid any coalescence effect at substrate level, named "short deposition", was also prepared in order to investigate the size distribution of the NPs generated by the cluster beam. As will become clear in the next section, as a result of the above

conditions the NP densities were in the range $10^{12}$-$10^{13}$ cm$^{-2}$. For clarity we should remind that

the film load is related to the equivalent film thickness (equivalent to that of a

uniform/atomically flat thin film) and to the NP film properties according to the following

equalities:

$$load = \rho \times thickness = \rho \times \frac{1}{A}\sum_{i}Vol(NP_{i}) = \rho \times \sigma \times \langle Vol(NP)\rangle \qquad (1)$$

where $\rho$ is the density of the material, A is the area of the substrate where the NPs are being

deposited, Vol indicates the volume, $<>$ is the mean value operator and $\sigma$ is the areal density of

the NPs. The first equality holds for any thin film while the subsequent 2 are specialized for the

case of NP films. For example, A 1 nm thick Au thin film corresponds to a load of 1,93 µg/cm2.

A FEI CM20 TEM operating at an accelerating voltage of 200kV was utilized for TEM

study of the samples. NPs' shape factors and size distributions (diameter) have been extracted

from the TEM images by analyzing the area of each NP. NPs' coverages have been calculated

from the TEM images as the ratio between the total area of all NPs appearing in the image and

the imaged area. Note that the TEM images presented in this manuscript are only a small

representative sample of all the TEM images (at different magnification levels) that have been

acquired and analyzed in order to validate the above analyses.
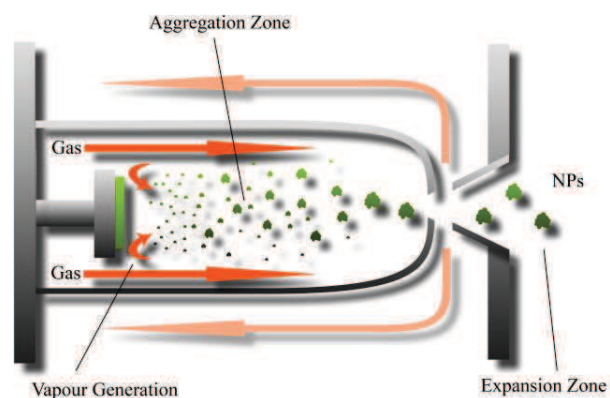
**Figure 1. Schematic of the cluster beam used in this work to fabricate Au NPs at room temperature.**

**Table 1. <mark>The samples considered in this work, fabricated by varying the deposition time (the corresponding NP load values are also shown)</mark>**

| *Sample* | short deposition | A | B | C | D |
|---|---|---|---|---|---|
| *Deposition time (min)* | 2 | 25 | 50 | 75 | 100 |
| *NPs Load (µg/cm², Au)* | 0.01 | | 0.209 | 0.532 | 0.810 | 1.231 |

## 3    Results

Figure 2 shows TEM plane view images of the as prepared samples A-D. The statistical analysis of the lateral size distributions, shown in the insets, suggests that the average NP size increases substantially with load while the NP areal density remains relatively unchanged. Contrary to this, the size dispersion appears to increase with increasing Au load. These observations are graphically summarized in Figure 3a. The NP density (black line) increases from sample A to sample B (maximum) and then decreases for samples C and D. The NP lateral size (red line) also increases - here it would seem that a linear relation with the load fits well the data points but as we will show later the situation is more complex than that. After extrapolating the data to 0, it is also possible to infer the average diameter of the NPs generated from the

cluster beam which is estimated to be around 1.3-1.4 nm. Figure 3b shows the NP film coverage of the substrate as a function of Au load. The NP film coverage was calculated directly from the TEM images and is defined as the ratio of the area occupied by the NPs to the total area of the imaged region. The results show that the NP film coverage initially increases in a linear fashion with increasing Au load, and then saturates at a coverage of 0.23-0.24. Interestingly, the TEM images show that for all samples the NPs are always in very good approximation circular and well separated from one another i.e. it is very hard to find two NPs in contact to each other.

Clearly, the NP density of the four samples presented up to this point is relatively high and therefore it is highly probable that already at sample A condition, some particles have coalesced with others to produce larger particles. For this reason and in order to establish the size characteristics of the Au NPs generated by the cluster beam, we have also carried out an additional deposition experiment which aimed to produce a very low Au NP density on the sample. This was achieved by utilizing the same conditions used for the previous four samples with the exception of the deposition time which was reduced to 2 min and led to a NP load of approximately 0.01 $\mu g/cm^2$ From this point onwards we will refer to this sample as "short deposition". Due to the very low areal NP density in this sample, the analysis required the acquisition of several TEM images in randomly chosen locations on the substrate, see Figure 4a-b. The Au NPs produced by the cluster beam generator were found to be predominantly of two sizes (Figure 4c): 0.9±0.1 nm and 1.3±0.1 nm in diameter. It is worth noticing that the mean size of the distribution was found to be 1.40 nm, in excellent agreement, considering the experimental errors potentially involved, with the average diameter of the NPs generated from the cluster beam that was estimated previously from Figure 3a extrapolating the data to 0 load.
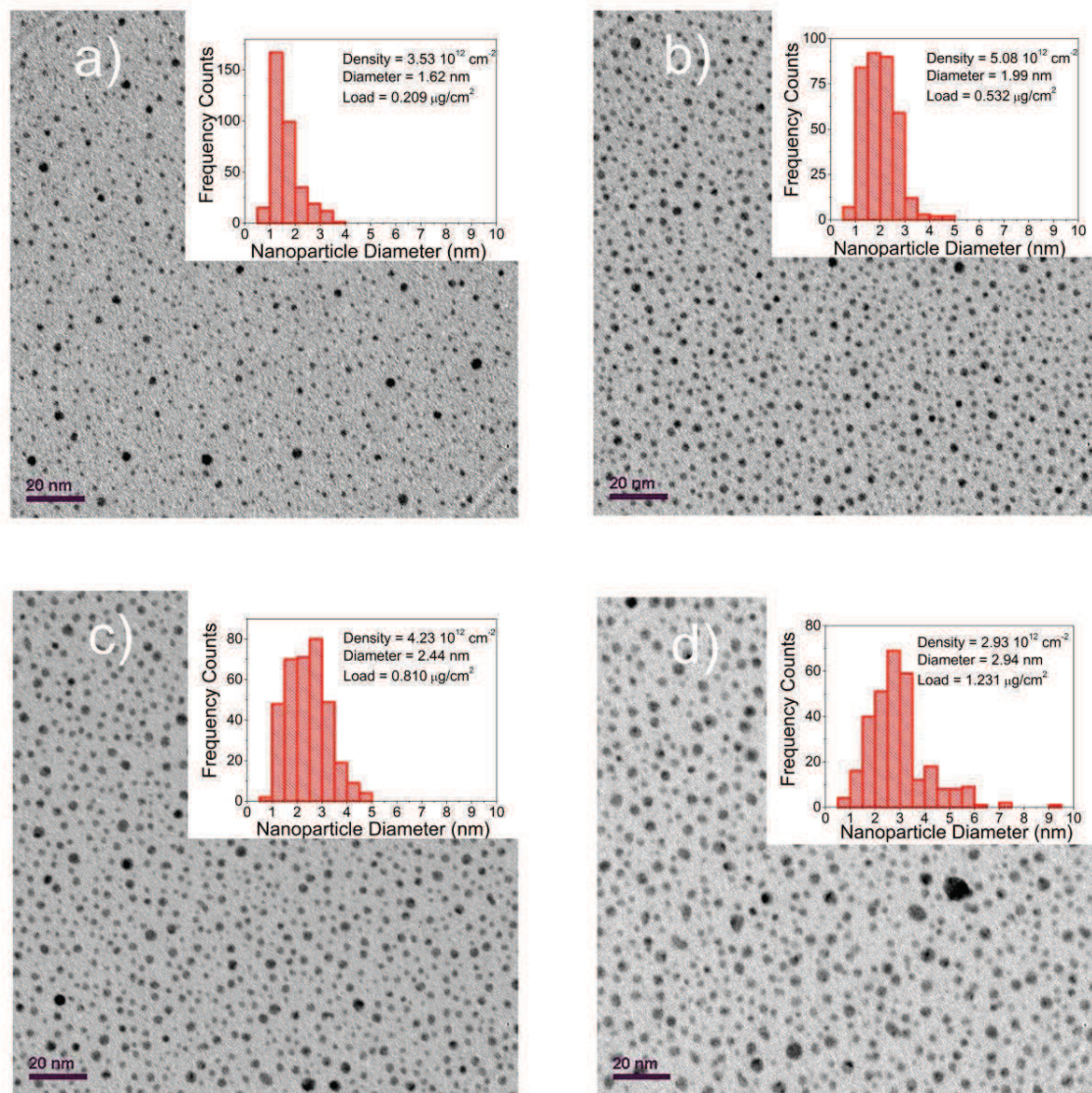
10

**Figure 2. Plan view TEM images and NPs distribution (bin size of 0.5 nm) for the four samples considered in this work. a) A (0.209 µg/cm$^2$), b) B (0.532 µg/cm$^2$), c) C (0.810 µg/cm$^2$) d) D (1.231 µg/cm$^2$). The bar corresponds to 20 nm, the imaged area is 176 nm x 176 nm .**
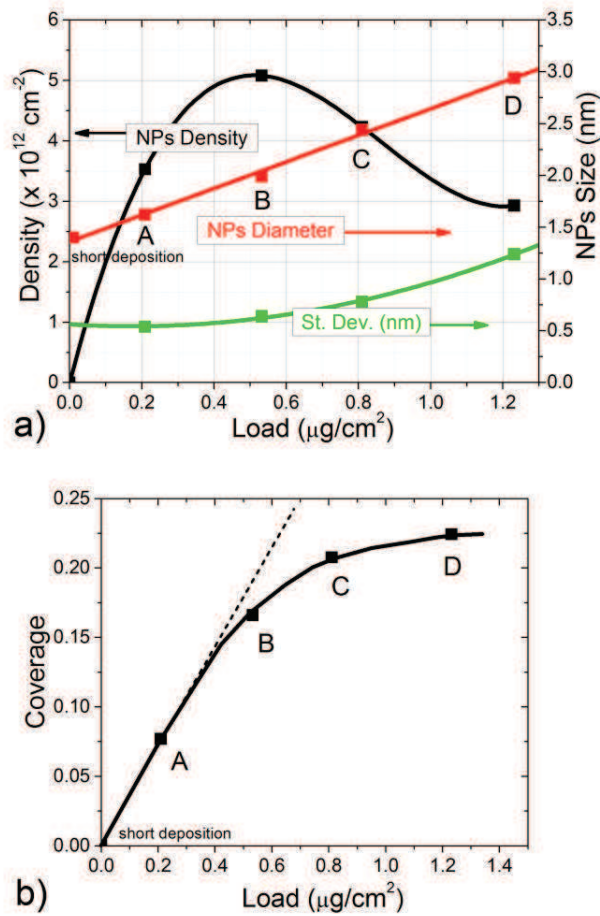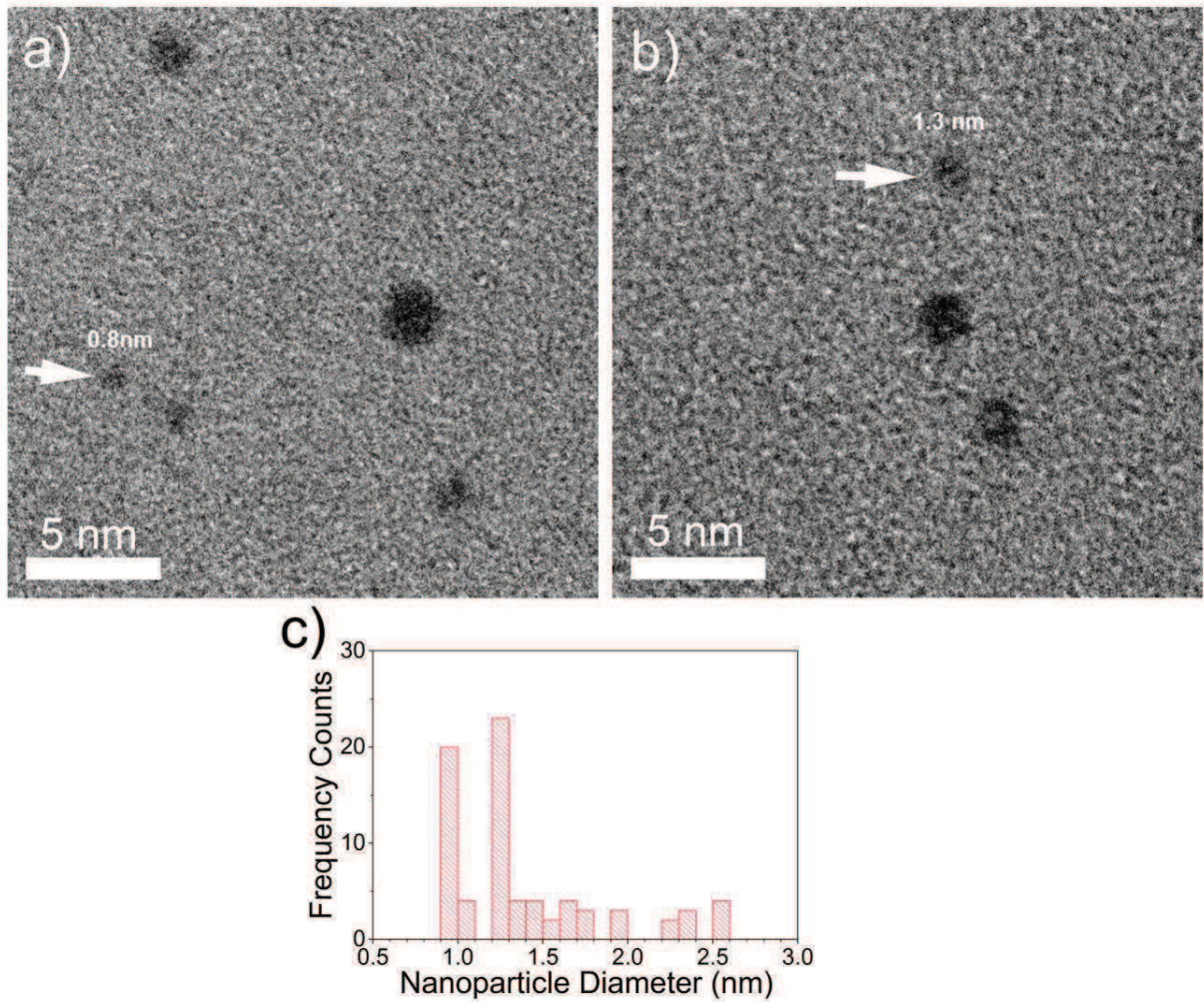
11

**Figure 3. a) Density and NP size plots as a function of Au loading. b) fraction of the surface of the sample covered by the Au NP film as a function of the load. The coverage increases linearly with the load nearly up to sample B and then shows a saturating behavior in C and D. (All data have been extracted from the TEM images shown in Figure 2)**

**Figure 4. Results concerning Au NPs deposited at very low areal density ("short deposition"): a), TEM images showing Au NPs of 0.8-0.9 nm b) TEM images showing Au NPs of 1.3 nm, c) Au NP diameter distribution (bin size of 0.1 nm) with the above two sizes clearly dominating over the others.**

## 4    Discussion

### 4.1    NP films growth kinetics

The results presented in **Figure 3**a seem to support the existence of two distinct regimes during the Au NP film growth that we will refer to as: "landing regime" and "coalescence regime". The landing regime dominates the very early stages of NP deposition (i.e. load say < 0.1 μg/cm$^2$ in such a way that the NP density is less than 1 10$^{12}$ cm$^{-2}$); the dominant nanocluster population on the substrate are Au NPs, as generated from the cluster beam generator, which land on the substrate in such a way that they are well isolated from other NPs and so they don't undergo any coalescence process at substrate level. On the other hand, the coalescence regime refers to a later stage in this process (i.e. load say > 0.5 μg/cm$^2$) that dominates when the NP density on the substrate is high enough in such a way that the NPs being deposited on the sample interact with the preexisting NPs and their coalescence is the dominant phenomenon taking place. Having in mind the above classification in two regimes, we could attempt here below to describe qualitatively what is happening in our samples. In the landing regime we can deduce that the mean NP diameter is constant and the NPs density varies linearly with the load. We have already shown in one of our previous works [52] that with small NPs and at low NPs densities, say <10$^{12}$ cm$^{-2}$, the NP density would vary linearly with the load (or deposition time). Furthermore, as it will become clear later in this work, both our theoretical model and simulation results support the above statements. As the load approaches 0.209 μg/cm$^2$ (sample A), a small fraction of NPs has already started coalescing with other NPs. This can be due to (i) the increased probability of an incoming NP hitting an existing NP on the substrate surface or/and (ii) the diminished distance between neighboring NPs. The appearance of coalescence at this point causes the mean NP size to increase while the NP density, although is still increasing, it

14

does so at a smaller rate (A-B region). As the Au load increases further, the coalescence phenomena become more prominent. As the Au load reaches 0.532 μg/cm$^2$ (sample B) the nanoparticle density goes through a maximum indicating that NP coalescence from this point onward is the key process governing the film growth. In this regime the NP diameter increases while the density decreases with increasing load (samples B-D). Interestingly, results that go along the lines of those discussed here were reported by Shyjumon et al. for the case of Ti nanoparticles on Si substrates [53].

Figure 3b shows a plot of the surface coverage as function of Au NP load where it is identifiable an initial linear behavior and a subsequent saturating behavior. In order to derive some useful insights from the surface coverage data we should take into account that i) the NP coverage, in the presence of coalescence processes, is a measure of the 2D lateral growth and ii) the load is an indirect measure of the volume of the Au deposited on the substrate. This means effectively that a linear dependency of the coverage vs Au NP load would indicate either a landing regime (no coalescence, NP diameter constant, NP density increasing linearly with load) or a coalescence regime with 2D lateral growth (NP diameter increasing with load, NP density either constant or decreasing with load). Conversely, any saturating behavior of the coverage with the load would indicate some coalescence with 3D growth (lateral + vertical growth). The experimental coverage data of the Au NPs seem to support the idea of an initial landing regime followed by a coalescence regime. Indeed up to a Au load of 0.532 μg/cm$^2$ (sample B) the coverage grows nearly linearly, which denotes a dominant landing regime (we can exclude lateral 2D growth at this early stage since the NP density nearly doubles when the load is doubled). In marked contrast, the coverage stays almost constant at approximately 0.23 between samples B and D, indicating a dominant coalescence regime with the 3D growth of the NPs.

15

**Coalescence of cluster beam generated sub-2 nm bare Au nanoparticles and analysis of Au film growth parameters**

It is well established that the relation between the feature size of the considered nanostructure and the film height (or load in this case) is given by the following equation:

$$< size > \propto thickness^{\frac{1}{z}}$$
(2)

with z being the dynamic scaling exponent (usually >1) (see Ref[29] and references therein). In order to provide further evidence in support of the existence of two growth regimes, we present in Figure 5 the log-log plot of the average nanocluster size vs. the load. We should remind that the load is proportional to the thickness of the film according to eq. (1). In other words the above mentioned log-log plot provides a direct way to highlight any power-like relation, as eq. (2), existing between the average nanocluster size and the load or thickness of the film. Two distinct growth regimes are indeed observed: the first one concerns the region up to sample B, and the second one concerns the region between samples B-D where the 1/z exponent is 0.47±0.01 (z=2.13). Regarding the former, taking into account that at very low load ("short deposition") the mean NP diameter is around 1.4 nm, the red dashed curved has been drawn on the plot in Figure 5 as an educated guess of the actual function representing the mean NP diameter vs load. This shows that at the very early stages of the deposition the 1/z exponent in eq. (2) should be 0 and then it should steadily increase attaining the value of 0.47 observed in the coalescence regime, as the load approaches the conditions used for sample B and then up to D. In order to stress the key differences between the B-D region and the one before sample B, in Figure 5 we have also drawn a straight line between A-B which would correspond to a 1/z exponent of 0.22. According to our educated guess curve, the 1/z exponent varies steadily in the landing regime so the above value should be regarded as the average 1/z exponent between A and B. It will soon become clear later in this work that our modeling and simulation results support the results shown in Figure 5.

16

The existing growth data/models in the literature all refer to the case of Au atoms being deposited on a substrate. For example, Ruffino et al. [29], by studying the RT film growth of Au atoms evaporated onto Si, have shown that, on a 2D surface, conservative systems (systems that conserve the number of nanoparticles on the substrate) should show z=4 (1/z=0.25) while non-conservative systems should present z in the range 1.2-1.7 (1/z = [0.59, 0.83]). The same authors were also able to produce evidence for the existence of four different growth regimes of the Au nanoclusters, each with a characteristic scaling exponent: 1) nucleation, 2) lateral growth, 3) coalescence and 4) vertical growth. Karoutsos et al [54] , by studying the RT film growth of sputtered Au onto oxidized Si substrates, reports a 1/z value of 0.41 concluding that the film growth mechanism is related to the diffusion of Au atoms. Ramalingam et al [55] by studying the growth of sputtered Pt on alumina substrates report results which agree with an initial nucleation model followed by a subsequent coalescence regime. They also provide a plot for the NP density as a function of film thickness which is in excellent qualitative agreement with the one shown in Figure 3a. Similar evidence is provided by Iwamoto et al. [56] and Zhang et al [57]. Particularly the latter work, shows data concerning the evolution of nanocluster density and average nanocluster size as functions of the load that are in excellent qualitative agreement with the data presented herein.

However, it is worth noting that the aforementioned works, involve the deposition of Au atoms on the substrate via evaporation or sputtering. In this work the situation is very different as pre-formed NPs (clusters of many Au atoms) are deposited on the substrate. The scaling law represented by equation (2) involves quantities that are intrinsically independent from the building block being deposited, be it atom or nanocluster, as they refer generally to the average lateral size/diameter of the structures observed/formed on the substrate and the thickness of the

deposited film. In this framework, it does make sense to apply such scaling law also in our case, as we did in Figure 5. The question we would like to address now is though, how can we explain the fact that the 1/z exponent in our case goes from 0 up to 0.47? what type of processes are taking place at substrate level to make this possible?

## 4.2 Coalescence model for landed nanoparticles

To properly address those questions we should take into consideration several parameters like i) the shape of the landing NPs and ii) the shape of the NPs formed through coalescence and iii) the kind of coalescence processes taking place on the substrate.

### 4.2.1 Type of coalescence processes

the coalescence processes that could take place at substrate level are obviously many. For instance, the most basic process is the one represented by a NP landing on the substrate where it interacts with nothing else. Such process steadily increases the NP density without changing the NP size distribution. We define this process as a 1-0 process (read 1 to 0). The next simpler one is the one involving 1 oncoming NP and 1 NP on the substrate e.g. 1-1 processes (read 1 to 1). This process will produce 1 new NP but leaving the count of NP on the substrate unchanged (the NP density would remain constant). 1-2 processes would require the involvement of 1 oncoming NP and 2 NPs on the substrate, creating 1 new NP but actually resulting in the removal of 1 NP from the count on the substrate. Note that a 1-2 process and any 1-many process, doesn't require the interaction at exactly the same time of 1 oncoming particle and 2 or more NPs on the substrate but could be imagined also as a succession of 1-1 processes: 1-2 is equivalent to 1-1 followed by the interaction of the newly formed NP with another on the substrate. Someone could go on with 1-3, 1-4 etc. processes but we should also keep in mind that the probability of such processes may well be different (smaller generally) from the one of the simpler 1-1 or 1-2

18

processes. From the above arguments it becomes clear that 1-n processes (n>1) are those that are responsible for decreasing the density of NPs on the substrate.

### 4.2.2    NP shape and relation to film growth regime

Our TEM observations show that the Au NPs on the samples discussed in this work are very circular in plane view (the detailed analysis of the shape of the NPs is discussed in detail in the **supporting information, section 3**) which would indicate that their actual shape can only be a sphere, an oblate spheroid or a disk. It would seem reasonable at this point to speculate that initially the NPs are spherical and they remain so in the first stages of the growth (especially because NPs with lateral sizes as small as 1 nm or few nm as in this work have been shown to have spherical structures as their most stable configurations, **see supporting information** section 4 and references therein); as they coalesce/grow further they would slowly tend to degenerate into oblate spheroids; as these spheroids grow larger they would tend finally to assume a disk-like shape and would grow mainly laterally. The case of a coalescence process where the resulting NP is spherical could be regarded as the ideal case of a 3D growth scenario, the case of a coalescence process where the resulting NP grows only laterally and thus has a disk-like shape could be regarded as the ideal case of a 2D lateral growth while the case of a coalescence process where the resulting NP is an oblate spheroid could be regarded as an intermediate situation between the previous two. Here below we analyze the two limit growth cases of spherical and disk-like NPs.

### 4.2.3   Model for spherical NPs (3D growth) and disk like NPs (2D growth)

Assuming that the NPs are spherical at every stage of the film growth (3D growth) it is clear that in presence of only 1-0 processes, the thickness of the film would increase with increasing film thickness or load while the mean diameter of the NP would remain constant (the

19

exponent in eq.(2) would be 0). In presence of only 1-1 processes, Figure 6a, the value of the exponent in eq.(2) could be calculated by considering a situation where N identical oncoming NPs interact with N identical NPs on the substrate (equal diameter $D_0$) in 1-1 processes to produce N new NPs. The diameter of the new NPs and the film thickness would be given by ==(the volume of the new NP is $V_1 = V_0 + V_0 = 2 V_0 \rightarrow D_1^3 = 2 D_0^3$)==

$$\begin{cases} D_1 = D_0 \sqrt[3]{2} \\ thickness_1 = thickness_0 \times 2 \end{cases} \tag{3}$$

which at the n-th step would read

$$\begin{cases} D_n = D_0 \times \left( \sqrt[3]{2^n} \right) \\ thickness_n = thickness_0 \times 2^n \end{cases} \tag{4}$$

The above parametric equation provides, through few substitutions, the relation between the diameter of the NPs and the thickness of the film in the case of 1-1 processes, and it turns out that the exponent of equation (2) would be equal to 1/3 in this case. We could imagine to repeat this procedure for 1-2 or 1-3 processes and also do the same under the assumption that the NPs are not spherical but disc-like at every stage of the growth, see Figure 6b (2D lateral growth). Equations similar to equation (4) can be found also for NP density and coverage as shown in the **supporting information** section 1 (see also Figure S1). The expected 1/z exponents related to equation (2) are presented in Table 2, together with the exponents for the similar power-like relations concerning NP density and coverage. More details about the derivation of these parametric equations are provided in the **supporting information section 1**.

### ==4.2.4 Experiment vs Model==

**Coalescence of cluster beam generated sub-2 nm bare Au nanoparticles and analysis of Au film growth parameters**

From this analysis it becomes clear that the data shown in Figure 5 are compatible with the scenario of spherical NPs (3D growth). This conclusion can be supported by the following observations (concerning film thicknesses, or loads, in the range between samples B-D): (i) the NP density decreases, which means that only 1-n processes with n=1,2,3… dominate in this regime, (ii) the NP film coverage shows a saturating behaviour, (iii) the mean NP diameter grows in a power-like fashion with exponent 0.47. Considering that the 1-1 process would have an exponent of 0.333 for spherical NPs (3D growth) or 0.5 for disk-like NPs (2D growth), observation (iii) could either suggest 3D growth with dominating 1-1 processes and few 1-2, 1-3 processes (to account for the exponent mismatch) or a 2D growth with only 1-1 processes. The hypothesis of 2D growth though is unrealistic according to observation (ii) as because 1-1 processes in a 2D growth regime cannot account for the saturating behavior of the coverage. On the contrary, a 3D growth regime, dominated by 1-1 processes, with few 1-2, 1-3, 1-n processes would explain both (i) the decreasing NP density and (ii) the saturation of the NP coverage for increasing Au NP load. The former is explained by recalling that 1-2, 1-3, 1-n processes induce a net decrease of the number of NPs in the sample (see also Figure S1 in the **supporting information section 1**). The latter instead can be explained by combining the effect of two contributions: (i) when coalescence starts we move from dominating 1-0 processes to dominating 1-1 processes and the NP coverage growth rate would decrease from 1 dec/dec (linear coverage vs thickness relation) to 2/3 dec/dec (sublinear coverage vs thickness relation that would lead to a plateau-like situation); (ii) in the coalescence regime there will be few 1-2, 1-3, 1-n processes that contribute to further decrease the coverage (if were dominating would exponentially reduce the NP coverage as shown in Figure S1 in the **supporting information section 1**).

21

The experimental results presented so far fit well a 3D growth kinetic model where the actual processes dominating the coalescence regime in the region between samples B-D are mainly 1-1 processes with a small amount of 1-2 or 1-3. On the other hand, during the initial "landing regime" up to sample B, the dominating process is the 1-0 ($1/z$ exponent equal to 0) with 1-1 and higher processes becoming more and more probable as the conditions of sample B are approached ($1/z$ exponent slowly increasing from 0 toward 0.47) providing support in this way to the educated guess represented by the red dashed curve in Figure 5.
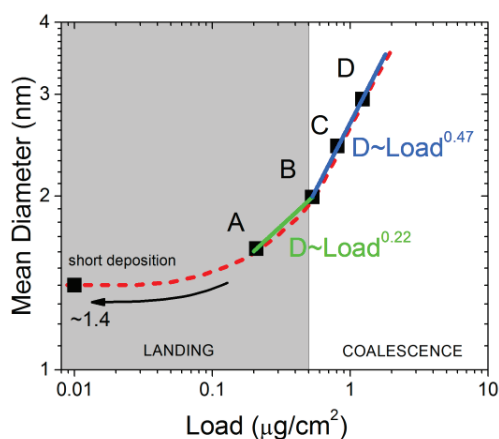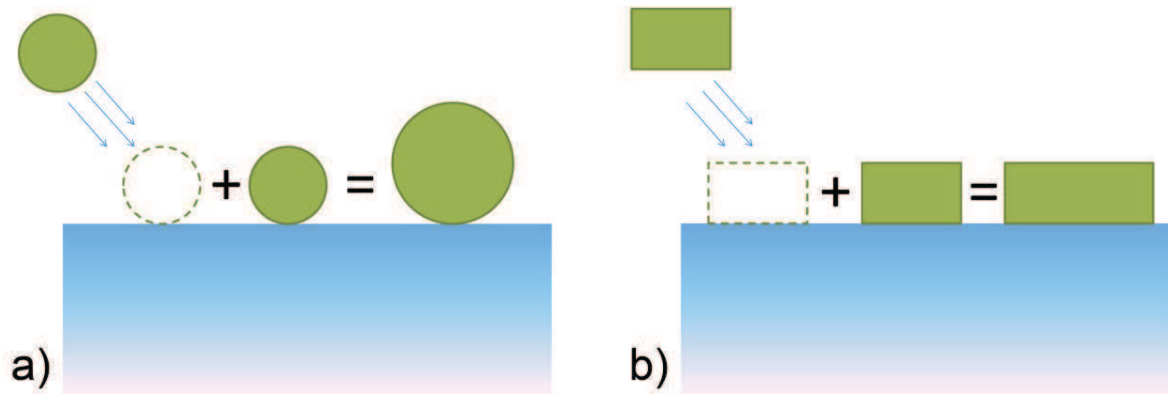


**Figure 5. log-log plot of the Au NPs' mean diameter as a function of the load (or film thickness) showing the existence of a two phase growth process. The B-D data points are well fitted by a straight line. The region before B presents a different trend. The red dashed curve represents an educated guess of the actual function that could join our data points, this is supported by our theoretical modeling and simulation work in the manuscript. To further stress the difference between the two regions we have drown a straight line between A and B which requires a $1/z$ exponent equal to 0.22.**

**Figure 6. schematic representation of the 1-1 process for a) spherical NPs (3D growth), b) disk-like NPs (2D lateral growth). Note that the disk-like assumption represents a limit idealized condition that simplifies the analysis for the 2D lateral growth scenario but it does not imply nor requires that the NPs generated by the cluster beam are also disk-like; actually the shape of the NPs doesn't really matter in this case while the only true requirement is that the NPs conserve their height constant throughout all stages of the growth (at least during the very first stages of growth as those studied in this work)**

**Table 2. Values of the 1/z exponent in equation (2) and the exponent for any power like relation existing between NP density or coverage with the film thickness under the assumption of either spherical or disk-like NPs for several coalescence processes that may take place at substrate level: 1-0 (i.e. no coalescence just NP deposition), 1-1 (1 oncoming NP coalesces with 1 NP on the substrate), 1-2 (1 oncoming NP coalesces with 2 NPs on the substrate) etc. If the relation is not power-like but rather exponential, as indicated in some cases here below, the + and – signs indicate whether the exponential function is monotonic increasing or decreasing respectively.**

| *process* | NP diameter vs thickness | | NP density vs thickness | | NP coverage vs thickness | |
|---|---|---|---|---|---|---|
| | 3D growth (Spherical NPs) | 2D growth (Disk-like NPs) | 3D growth | 2D growth | 3D growth | 2D growth |
| *1-0* | 0 | 0 | 1 | 1 | 1 | 1 |
| *1-1* | $\frac{1}{3} \approx 0.333$ | 0.5 | 0 | 0 | $\frac{2}{3} \approx 0.666$ | 1 |
| *1-2* | +exponential | +exponential | -exponential | -exponential | -exponential | 0 |
| *1-3* | +exponential | +exponential | -exponential | -exponential | -exponential | 0 |

## 4.3  Magic numbers

The experimental NP size distributions presented earlier show several clear sharp peaks when we look at their fine structure, which could be related to the appearance of more stable NPs i.e. magic number clusters. In order to correlate the NP diameters observed in this work with Au magic numbers, we gathered from the literature relevant data about Au clusters with a magic number of atoms spanning the range 13-40000, that was then used to create an interpolating

function able to correlate Au NP diameters with Au cluster size in atoms. This relation was then used to identify Au magic numbers in the experimental distributions of NP diameters found in this work. The full details of this procedure are discussed in the **supporting information section 4** and the result of this identification process is shown in Figure 7 where we present for each sample the identified peaks, their relative intensity (calculated as the % ratio between the counts "under" the peak and the total number of counts) and the position of relevant Au Magic numbers for peak matching purposes. All identified peaks match reasonably well an Au magic number. The main remark we should make at this point is that from this analysis it is clear that more than 95% of NPs generated by the cluster beam (short deposition sample) correspond to stable Au magic numbers and coalescence at substrate level is responsible for the creation of Au magic numbers much larger than those generated by the cluster beam. The analysis presented in Figure 7 suggests that coalescence is actually responsible for the evolution of the relative intensity of every peak as the NP load increases. $Au_{20}$ is very intense in the short deposition sample but its intensity quickly drops to 0 as we approach the conditions of sample B.  A similar behavior is observed for $Au_{55}$ and in a less dramatic way also for $Au_{92}$, $Au_{147}$, $Au_{181}$($Au_{200}$). Apparently $Au_{307}$ represents a border case as its intensity initially increases from A to B and then decreases slightly in C and D. The identified clusters above 307 all seem to boost their intensities as we move from A to D. Characteristic example is $Au_{561}$ which is a faint peak in sample A, representing just the 3% of the total NP population, and it grows to more than 22% in sample D.

We would like to remark that interestingly all the identified magic clusters match the geometrical shell closure of those polyhedra that are quasi-spherical e.g. dodecahedron, decahedron, etc. This result provides further support to the idea of a 3D growth of the NP film as the NPs are spherical at all stages of the film growth process (at least up to the conditions used

25

for sample D). More importantly, the results summarized in Figure 7 provide, to our knowledge, the first experimental evidence that magic number clusters are formed at substrate level through the coalescence of smaller NPs.
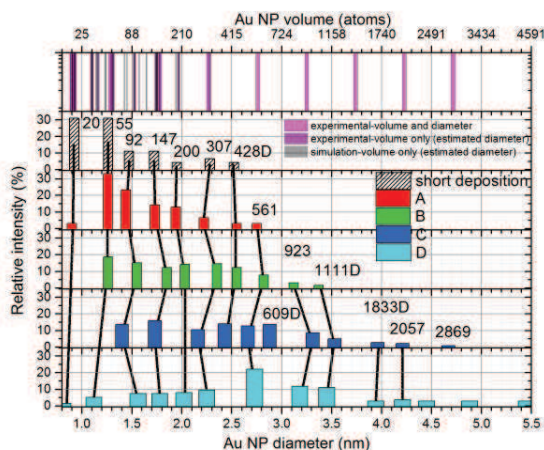


**Figure 7. Summary of identified peaks. The vertical lines in the top row represent identified magic number clusters that are shown in this graph to facilitate the peak identification process. The identified magic numbers in our samples are indicated next to the corresponding peak at its first occurrence as we move from "short deposition" to sample D. The black thick lines are guides to the eye aimed at indicating peaks corresponding to the same magic numbers over different samples. The peaks marked with a D correspond to known decahedron shell closures. See supporting information for more details**

## 4.4 Nearest neighbor analysis-Coalescence mechanism

Au NPs may coalesce with other neighboring NPs when the nearest neighbor distance (NN) is relatively small. The entire process that we call coalescence, especially for the case of spherical Au NPs, could be divided into three sub-processes: (i) attractive forces induce the NPs to come in close proximity and in contact eventually, (ii) an increasingly thicker bridge of Au atoms is formed between the two NPs that have become a single entity, (iii) Au atoms on the newly formed NP redistribute in order to minimize the configurational energy [58]. While (ii) and (iii) could be regarded as belonging to the broad research field relating to Au magic numbers and

Au nanocluster stability (see **supporting information,** section 4), process (i) is of particular interest because 1) the literature is quite scarce yet on this matter and 2) the mechanisms responsible for this process to occur could be quite diverse [58].Regarding the latter point, some examples could be: Electrostatic forces generated by charge transfer [48], electrostatic forces generated by dipole moments interaction mediated by plasmons [59,60], London, van der Waals, Casimir and oscmotic forces [61,62,63]. Generally speaking process (i) should require the involvement of two forces, a long range one and a short range one. By taking into consideration the fact that in cluster beam deposition the speed of the landing nanoparticles can be of the order of tens or hundreds m/s[64,65], someone could anticipate that the nanoparticles upon landing would have enough excess kinetic energy to allow them to slightly move around the landing site until this energy is fully dissipated by friction. In this working scenario process (i) could originate simply by short range forces. Although it is beyond the scope of this work to determine the mechanism originating process (i), regardless of the physical process several reports in the literature seem suggesting that depending on NP system, substrate, etc, there is a critical minimum nearest neighbor distance (NNc) such that anything below that critical value will coalesce [48,58,61].

NN analysis of the TEM images discussed in this work (see **supporting information** section 2 for the full analysis) highlights the unique self-organization properties of such small Au NPs in creating films that in the coalescence regime show stable edge-to-edge NN characteristics with 1) maximum NN of 4.1 nm, 2) mean NN of 1.4 nm, 3) minimum or critical NN, or simply NNc, of 0.5-0.4 nm  (Figure 8a). There are two remarkable results that is worth noticing. Firstly, in the coalescence regime the mean NN distance is 1.4 nm which is equal to the mean NP size

generated by the cluster beam. Secondly, an NNc of 0.5 nm is in good agreement with a recent work on Au NPs deposited on carbon substrates by Neng et al. [58]. Lastly, it is meaningful to note that Au NP films like those in this work seem to posses quite unique self-organization properties (see also [66]) that have not been observed with other metallic NP films made out of materials other than Au (like Ni, Ti, Si, Pt, etc) also fabricated via cluster beam deposition (see Figure S12-S14 in the **supporting information section 3**).

### 4.4.1    Simulation results

In order to gain insight into the coalescence phenomenon, we have developed a simulation program of the deposition process of the Au NPs generated by our cluster beam generator using Mathematica. The simulation is based on the following five simple assumptions: 1) the film growth is 3D, 2) the NPs being deposited have a size distribution that is the one obtained experimentally from the "short deposition" sample, 3) the NPs travel in straight line with an approach angle of 45° respect to the substrate, 4) the NPs in absence of any external force would stop on the point they land on the substrate, 5) NPs closer than a certain critical distance NNc would coalesce. It is worth noting that given the innate complexity of the phenomena presented in this work, some of the above assumptions should be regarded as simplifying, zero-order, approximations that allow us to get an initial insight into the coalescence processes taking place. We recognize that an in depth simulation of the process would be well beyond the scope of this work. Someone could for example discuss the situation where assumption 4 is dropped and we assume that all landing nanoparticles travel a certain distance over the substrate before coming to a stop. Another even more realistic assumption could be to relate the travelled distance to the momentum of the landing particle (relate the distance to the mass of a NP, if we assume that all particles have the same speed at landing). The comparison of

28

the experimental and simulation results has been done using as reference the (macroscopic) behaviour observed for NP density, NP coverage and NP mean diameter vs film load. It should be remarked that this simulation tool has been constructed to test few simple scenarios only, as a full detailed modeling of all possible phenomena would have been beyond the scope of this work.

The first simulated scenario is the one with NNc constant and equal to 0.4 nm with no other process taking place (Figure 9a-c, black curve). This condition failed to reproduce the experimental results, especially the part concerning the coalescence regime (samples B-D). Remarkably, the simulation results improved drastically by keeping NNc constant as above and adding into the simulation a random walk of the NPs at substrate level with width of 0.05 nm, see Figure 9a-c red curve. The addition of mobility of the NPs at substrate level seems not only to capture the experimental results in the landing regime (A-B) but to some extent also those in the coalescence regime (B-D) and definitely provides a huge improvement over the situation with no random walk. The addition of some sort of mobility of the NPs in our simulation is strongly supported by existing literature. According to Jensen et al [67] and references therein, small gold nanoclusters on carbon substrates move on the substrate in a Brownian-like fashion with diffusion coefficients from $10^{-8}$ cm$^2$/s down to $10^{-15}$ cm$^2$/s. The third and last simulated scenario was the one where the condition of a constant NNc is dropped and NNc is actually a fitting function that depends on some parameters relevant to the deposition process. Among the different NNc functions tested, the one that provided the best match is a parabolic function of the size difference between the size of a given NP and the size of its nearest neighbor one (NN NP), as shown in eq. 5:

29

$$NNc(\Delta) = 0.4nm + 0.4 \times \Delta + 0.2nm^{-1} \times \Delta^2$$
$$\Delta = |NPsize - NN\_NPsize|$$

(5)

where "NPsize" is the diameter of the NP just landed on the substrate and "NN_NPsize" is the

diameter of the NN NP to the one just landed. In Figure 9d is shown a plot of this function while

in Figure 9e-f are shown two snapshots of the simulation corresponding to the conditions of

sample B and D respectively. While it is unrealistic at this stage to say whether this scenario has

a physical meaning or not, it is worth comparing Eq. 5 with the corresponding NN and $\Delta$ values

extracted from the experimental data as shown in Figure 9d. The solid black line representing

NNc from eq.5 clearly has experimental data points above and below it. Ideally, if eq.5 is

physically meaningful, the experimental data points should all lie above the solid black curve

which doesn't seem the case here but it is remarkable to note that there are just ~80 data points

out of 935 (8%) that actually lie below the line represented by eq. 5.

These simulation results indicate that a constant NNc of 0.4 nm with the addition of

mobility of the NPs at substrate level could be the right direction to go in order to fully model the

film growth and coalescence processes in these films. It is though noticeable the complexity of

what happens in the coalescence regime, demonstrated on one hand by the discrepancy between

the above simulation result and the experimental data (Figure 9a-c red curve) and on the other

hand by the fact that in order to fully capture the experimental results NNc should not be kept

constant but should be a function of some NP film parameters. We could speculate that the latter

could be the indication that attractive forces with an innate non-linear nature and with a strong

dependence from the NPs size may be at the heart of the growth and coalescence processes in

these films [48,59-63].

30
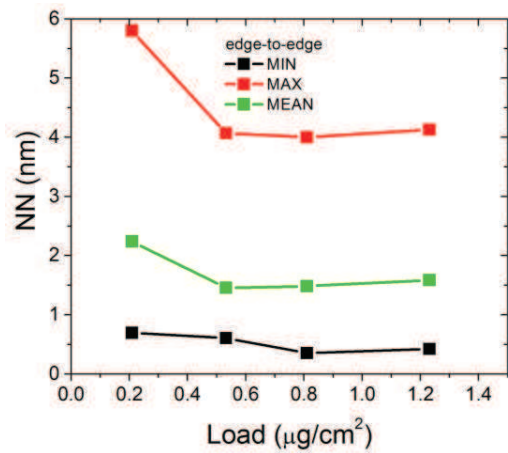
**Figure 8. Evolution with the NP load of the min, max and mean NN distance (edge to edge). Remarkably, the maximum NN is larger in sample A (landing regime) than in the other samples B-D (coalescence regime) while the minimum NN observed is always around 0.4-0.5 nm.**
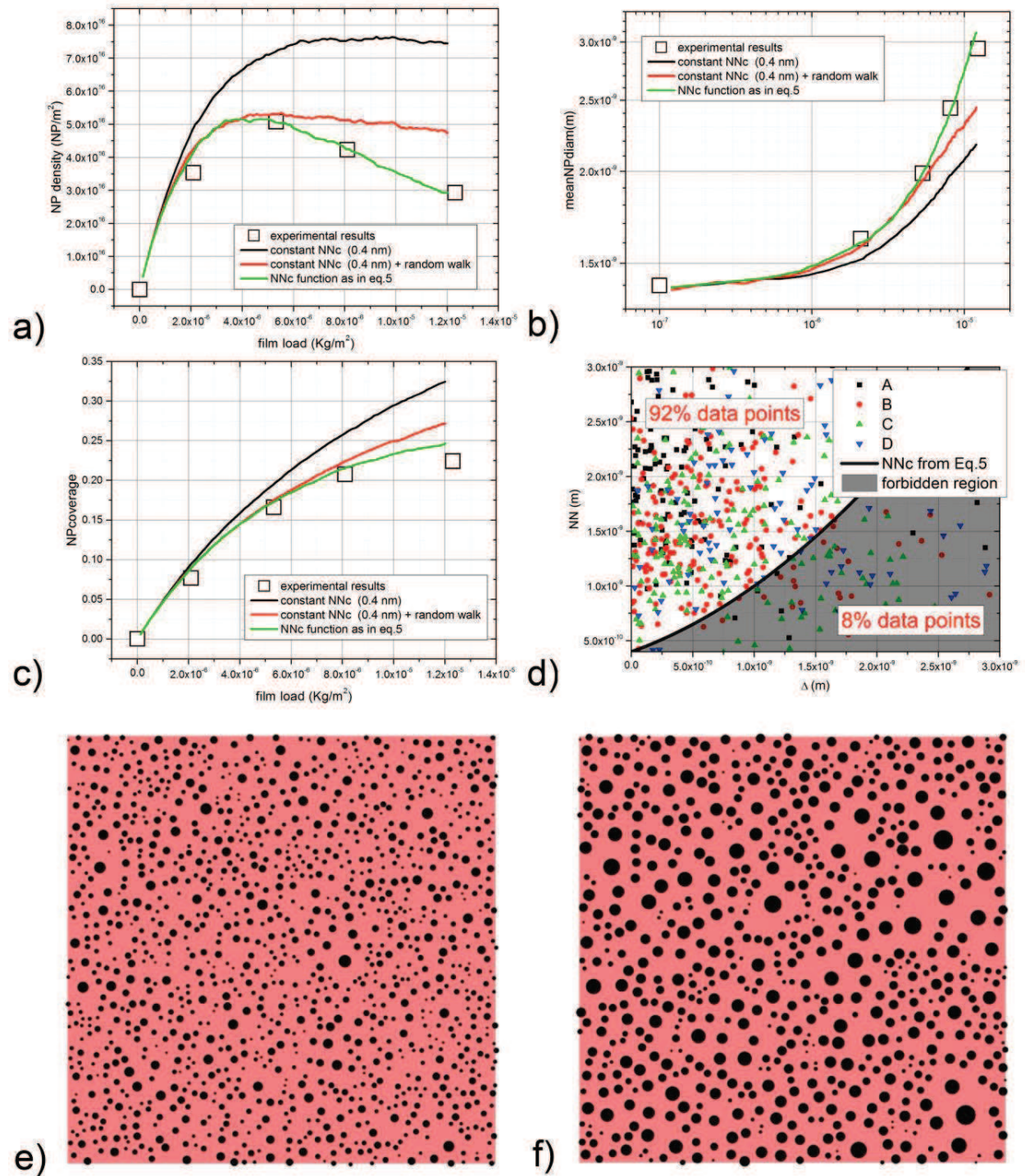
**Figure 9. a)-c) Comparison between simulation results (solid lines) and experimental data (square symbols) for the major macroscopic parameters characterizing the film growth: a)**

**NP density, b) mean NP size and c) NP coverage. The simulation results represented by the solid lines are obtained by: keeping NNc constant at 0.4 nm (black curve), assuming NNc constant and introducing random walk with constant width at 0.05 nm (red curve), best match using eq.5 (green curve). In d) is shown the graph of eq.5, the function relating the critical NN distance NNc with the size difference of two nearest neighbor NPs that was chosen in order to achieve the excellent match between experimental data and simulations (green line in a-c). Experimental data is also shown for comparison purposes. According to the definition of eq.5 given in the text, the region under the black curve should be a forbidden region for our system; it is remarkable that only 8% of all experimental data points fall in this region. e)-f) simulation snapshot at sample B and D conditions, respectively, using the best matching simulation conditions (imaged area of 150 nm side)**


## Conclusions

In this work was presented the film growth study of cluster beam generated Au NPs with

1.3-1.4 nm average diameter soft landing at room temperature on a carbon substrate and with

areal densities approaching $10^{13}$ cm$^{-2}$. The growth of Au nanoclusters through the coalescence of

Au NPs soft-landing on the substrate was investigated by TEM analysis of samples at increasing

Au load, in the range 0-1.2 μg/cm$^2$. The evolution of the nanoparticle lateral size and the nearest

neighbor distance at increasing NP load values support very well the argument of an initial

"landing regime" (samples A-B) followed by a coalescence regime (samples B-D). The film

growth during the coalescence regime is 3D with a dynamic scaling exponent z of 2.13.  The

statistical analysis of the TEM images revealed on the one hand that the cluster beam generator

produces a population of NPs that is clearly dominated by the gold cluster with magic number 20

and 55 and on the other hand that upon deposition on the substrate, the NPs coalesce with

neighboring ones allowing for the appearance of Au clusters with larger magic numbers e.g. 561

at expenses of the smaller clusters.  Experimental and simulation results provided insight into the

coalescence mechanism and provided strong evidence that the NPs investigated in this work

coalesce when the nearest neighbor distance is below a critical mark. The critical distance is at

its minimum 0.4-0.5 nm. It is still unclear whether it is constant or not although the best matching simulation results seem to point to a superlinear dependence from the NP size difference between two neighboring candidate coalescing NPs..

## Acknowledgements

## References

[1] G. Baffou and R. Quidant Chem. Soc. Rev., 2014, 43, 3898-3907

[2] P. Johnston, N. Carthey, G. J. Hutchings J. Am. Chem. Soc. 2015, 137, 14548−14557

[3] A. Urban, T. Pfeiffer, M. Fedoruk, A. Lutich and J. Feldmann, ACS Nano, 2011, 5, 3585–3590

[4] L. A. Lane, X. Qian, S. Nie Chem. Rev. 2015, 115, 10489−10529

[5] L. C. Grabow and M. Mavrikakis Angew. Chem. Int. Ed. 2008, 47, 7390 – 7392

[6] G. J. Hutchings, M. Brust and H. Schmidbaur, Chem. Soc. Rev., 2008, 37, 1759–1765.

[7] H. Li, L. Li, A. Pedersen, Y. Gao, N. Khetrapal, H. Jónsson, X. C. Zeng , Nano Lett., 2015, 15 (1), pp 682–688

[8] Charles T. Campbell Science, Vol. 306, Issue 5694, pp. 234-235 (2004)

[9] M. Turner, V. B. Golovko, O. P. H. Vaughan, P. Abdulkin, A. Berenguer-Murcia, M. S. Tikhov, B. F. G. Johnson, R. M. Lambert, Nature 454, 981-983, (2008).

[10] G. J. Hutchings, M. Haruta, Appl. Catal. A: General 291 2–5, (2005).

[11] M. S. Chen, D. W.Goodman, Science 2004, 306, 252-255.

[12] M. Haruta, T. Kobayashi, H. Sano, and Yamada, Chem. Lett., vol. 10, pp. 405–408, 1987.

[13] M. D. Hughes, P. Jenkins, P. McMorn, P. Landon, A. F. Carley, G. A. Attard, G. .J.Hutchings, F. King, H. Stitt, P. Johnston, K. Griffin, C. J. Kiely, Nature, (2005), 437, 1132-1135.

**Coalescence of cluster beam generated sub-2 nm bare Au nanoparticles and analysis of Au film growth parameters**

[14] M. T. Alotaibi, M. J. Taylor, D. Liu, S. K. Beaumont, G. Kyriakou, Surf. Sci. (2015) doi:10.1016/j.susc.2015.10.039

[15] P. Landon, J. Ferguson, B. E. Solsona, T. Garcia, A. F. Carley, A. A. Herzing, C. J. Kiely, S. E. Golunski and G. J. Hutchings, Chem. Commun., 2005, 3385.

[16] G. Kyriakou, S. K. Beaumont, S. M. Humphrey, C. Antonetti and R. M. Lambert ChemCatChem 2010, 2, 1444 – 1449

[17] S. K. Beaumont, G. Kyriakou, R. M. Lambert  J. Am. Chem. Soc. 2010, 132, 12246–12248

[18] A. Corma and P. Serna, Science 2006, 313, 332.

[19] T. Fujigaya, C. Kim, Y. Hamasaki, N. Nakashima, Scientific Reports 6, 21314 (2016)

[20] Dawn M. Wells,a  Giulia Rossi,b  Riccardo Ferrandob and  Richard E. Palmer Nanoscale, 2015,7, 6498-6503.

[21] H. Tsunoyama, T. Tsukuda J. Am. Chem. Soc., 2009, 131, 18216–18217

[22] H. Li, L. Li, A. Pedersen, Y. Gao, N. Khetrapal, H. Jónsson, X. C. Zeng, Nano Lett. 2015, 15, 682−688

[23] F. Baletto, R. Ferrando Rev. Mod. Phys., 77, 2005, 371-423

[24] E. Verrelli G. Galanopoulos, I. Zouboulis, D. Tsoukalas, J. Vac. Sci. Technol. B 31(3), 032204-1 (2013)

[25] N Vandamme, E Janssens, F Vanhoutte, P Lievens, C VanHaesendonck, J. Phys.: Condens. Matter 15 (2003) S2983–S2999

[26] H. Haberland, M. Karrais, M. Mall and Y. Thurner, Journal of Vacuum Science & Technology A: Vacuum, Surfaces, and Films 10 (5), 3266-3271 (1992).

[27] Yves Huttel (Editor), Gas-Phase Synthesis of Nanoparticles, ISBN: 978-3-527-34060-6, Wiley

[28] S. F. Hu, R. L. Yeh, and R. S. Liu, J. Vac. Sci. Technol. B 22, 60 (2004)

[29] F. Ruffino and M. G. Grimaldi, J. Appl. Phys. 107, 104321 (2010)

[30] V. Resta, C. N. Afonso, E. Piscopiello, G. Van Tendeloo, Phys. Rev. B 79, 235409  2009

[31] V. L. De Los Santos, D. Lee, J. Seo, F. L. Leon, D. A. Bustamante, S. Suzuki, Y. Majima, T. Mitrelias, A. Ionescu, C. H.W. Barnes, Surface Science 603 (2009) 2978–2985

[32] A. Iwamoto, T. Okazawa, T. Akita, I. Vickridge, Y. Kido, Nuclear Instruments and Methods in Physics Research B 266 (2008) 965–971

[33] G. Oskam, P. C. Searson, Journal of The Electrochemical Society, 147 (6) 2199-2205 (2000)

[34] C. Lee,  J. Meteer,  V. Narayanan,  E. C. Kan, Journal of Electronic Materials (2005), Volume 34, Issue 1, pp 1-11

[35] N Vandamme, E Janssens, F Vanhoutte, P Lievens1 and C VanHaesendonck, J. Phys.: Condens. Matter 15 (2003) S2983–S2999

[36] Ignacio López Salido, PhD dissertation, Konstanz University (2007), available online at http://www.ub.uni-konstanz.de/kops/volltexte/2007/2707/

[37] K. Baeg, Y. Noh, H. Sirringhaus, D. Kim, Adv. Funct. Mater. (2010), 20, 224–230

[38] T. Okazawa, M. Kohyama, Y. Kido, Surface Science 600 (2006) 4430–4437

[39] A. Rota, A. Martinez-Gil, G. Agnus, E. Moyen, T. Maroutian, B. Bartenlian. Me´gy, M. Hanbu¨cken, P. Beauvillain, Surface Science 600 (2006) 1207–1212

[40] S. Peli, E. Cavaliere, G. Benetti, M. Gandolfi, M. Chiodi, C. Cancellieri, C. Giannetti, G. Ferrini, L. Gavioli and F. Banfi, The Journal of Physical Chemistry C 120 (8), 4673-4681 (2016).

[41] G. Benetti, E. Cavaliere, A. Canteri, G. Landini, G. M. Rossolini, L. Pallecchi, M. Chiodi, M. J. V. Bael, N. Winckelmans, S. Bals and L. Gavioli, APL Materials 5 (3), 036105 (2017).

[42] E. Cavaliere, S. De Cesari, G. Landini, E. Riccobono, L. Pallecchi, G. M. Rossolini and L. Gavioli, Nanomedicine: Nanotechnology, Biology and Medicine 11 (6), 1417-1423 (2015).

[43] C. Minnai and P. Milani, Applied Physics Letters 107 (7), 073106 (2015).

[44] F. Borghi, C. Melis, C. Ghisleri, A. Podestà, L. Ravagnan, L. Colombo and P. Milani, Applied Physics Letters 106 (12), 121902 (2015).

[45] G. L. Celardo, D. Archetti, G. Ferrini, L. Gavioli, P. Pingue and E. Cavaliere, Materials Research Express 4 (1), 015013 (2017).

[46] A Majumdar, M Ganeva, D Kopp, D Datta, P Mishra, S Bhattacharayya, D Ghose, R Hippler, Vacuum 83 (2009) 719–723

[47] M DiVece, N P. Young, Z Li, Y Chen, and R E. Palmer, Small 2006, 2, No. 11, 1270 – 1272

[48] D. B. Pedersen and S. Wang, J. Phys. Chem. C 2012, 116, 3258−3265

[49] A. Downard, E. Tan, S. Yu, New J. Chem., 2006, 30, 1283–1288

[50] K. Hu, S. Plant, P. Ellis, C. Brown, P. Bishop, R. Palmer, J. Am. Chem. Soc. 2015, 137, 15161−15168

[51] E. Verrelli, D. Tsoukalas, Solid-State Electronics, 101,(2014), 95-105

[52] J. Tang, E. Verrelli and D. Tsoukalas, Nanotechnology 20 (36) (2009).

[53] I. Shyjumon, M. Gopinadhan, C. A. Helm, B. M. Smirnov and R. Hippler, Thin Solid Films **500** (1), 41-51 (2006).

[54] V. Karoutsos, M. Toudas, A. Delimitis, S. Grammatikopoulos, P. Poulopoulos, Thin Solid Films 520 (2012) 4074–4079

[55] B Ramalingam, S Mukherjee, C J Mathai, K Gangopadhyay, S Gangopadhyay, Nanotechnology 24 (2013) 205602

[56] A. Iwamoto a, T. Okazawa b, T. Akita b, I. Vickridge c, Y. Kido, Nuclear Instruments and Methods in Physics Research B 266 (2008) 965–971

[57] L Zhang, F Cosandey, R Persaud, T E. Madey, Surface Science 439 (1999) 73–85.

[58] W. Neng, L. Shuang-ying, X. Jun, M. Martini, Nanotechnology 27 (2016) 205605

[59] A. Reyes-Coronado, R. G. Barrera, P.E. Batson, P.M. Echenique, A. Rivacoba, J. Aizpurua, Phys. Rev. B 82, 235429

[60] P.E. Batson, A. Reyes-Coronado, R.G. Barrera, A. Rivacoba, P.M. Echenique, J. Aizpurua, Nano Lett. 2011, 11, 3388–3393

[61] D. Li, M H Nielsen, J R I Lee, C Frandsen, J F Banfield and J J D Yoreo, Science (2012) 336 1014

[62] A. W. Rodriguez, F. Capasso and S. G. Johnson, Nat Photon **5** (4), 211-221 (2011).

**Coalescence of cluster beam generated sub-2 nm bare Au nanoparticles and analysis of Au film growth parameters**

[63] D. Garcia-Sanchez, K. Y. Fong, H. Bhaskaran, S. Lamoreaux and H. X. Tang, Physical Review Letters **109** (2), 027202 (2012).

[64] M. Ganeva, P. V. Kashtanov, B. M. Smirnov and R. Hippler, Vacuum 110 (Supplement C), 140-145 (2014)

[65] M. Ganeva, P. V. Kashtanov, A. V. Kosarim, B. M. Smirnov and R. Hippler, Physics-Uspekhi 58 (6), 579 (2015).

[66] G.E. Johnson, R. Colbyb, J. Laskina, Nanoscale, (2015), 7, 3491

[67] P. Jensen, A. Clément and L. J. Lewis, Computational Materials Science 30 (1), 137-142 (2004)